Development of a parameterized mechanical model of a chisel-edge grating ruling tool

Jirigalantu *, Xiaotian Li *, Xiaotao Mi, Kai Liu, Yuguo Tang

Changchun Institute of Optics, Fine Mechanics and Physics, Chinese Academy of Sciences, Changchun, 130033, China

A B S T R A C T

The parameterized mechanical model is proposed to optimize chisel-edge grating ruling tool parameters, eliminate corrugated grating lines, improve surfaces roughness of blaze plane, and reduce complex fabrication works such as step-by-step modification of tool guide angle. A mathematical model of force and torque between the diamond tool and the metallic film during the ruling process is deduced to realize optimized diamond tool geometrical parameter design. Then, grating ruling experiments are performed by tools with different guide angles of 75°, 95°, 115° and 135°, respectively. The experiments results agree well with the theoretical calculation value of force and torque. Experiments show that our proposed method is an effective way to solve the corrugated line and fluctuating problems on grating grooves, and can avoid complex and time-consuming technical operations such as step-by-step modification of tool guide angle. This illustrates the significance of our model for practical applications in the ruling of high-performance gratings.

© 2017 Elsevier Inc. All rights reserved.

1. Introduction

Diffraction gratings are regular arrays of lines, slits, grooves or variations of any optical property. They were first made in 1785 by Rittenhouse, but their scientific value was not fully appreciated until their reinvention by Fraunhofer in 1821 [1]. The ruling of a grating involves the extrusion and polishing of a metal coating on a grating substrate and the formation of stepped grooves after deformation [2], as shown in Fig. 1.

The quality of the extruded surface either side of a step affects the spectral orders, diffraction angles and diffraction efficiency of the grating. However, studies on the extruded forming of gratings have so far been mostly empirical in nature, and the theoretical study of the extruded forming of gratings is immature. For both academic knowledge and manufacturing, it is important to advance the systematic theoretical study of the extruding and polishing mechanism of the grating groove. The tool and film are the two primary objects in research on the extruding and polishing mechanism of the grating groove, and their interaction is the primary consideration in the study of the mechanism. Li [3], Li et al. [4] and Yang et al. [5] point out the importance of tool and film manufacturing technique respectively. Harrison [6], who performed researches on

the ruling of large gratings and echelles using the MIT-C engine, observed that eight of the ruled large gratings failed because of the unclear mechanism between the ruling tool and the film, and only four large gratings were successfully ruled from a total of eighteen gratings.

The extruding and polishing of a grating film mainly involves plastic deformation associated with a small nonlinear elastic deformation, and the deformation mechanism is thus complex. The groove has a certain amount of resilience after the grating ruling tool passes, and the groove shape is mainly determined by the specific tool geometry in addition to the mechanical properties of the film. Harrison [7] stated that the greatest difficulties in producing the desired groove shape would probably arise from natural strains in, and plastic flow of, the material being cut, and storage in it of residual elastic energy. Verrill [8,9] analyzed the effects of tool alignment and tool wear on groove shape.

A universally used grating ruling tool is the chisel-edge (namely roof-edge or double-ended) tool [10]. The working region of this tool comprises one point (tool tip), two surfaces (tool side faces) and three edges (one main edge and two side edges) ground on natural diamond. In the ruling of a grating, as the tool moves forward across the film, the main edge of the tool incises off the film first, the side face of the tool then extrudes and polishes the film, and the side edge finally shapes the groove of the grating.

Generally, the cross section of a grating groove is asymmetric relative to a vertical line that passes through the point of the
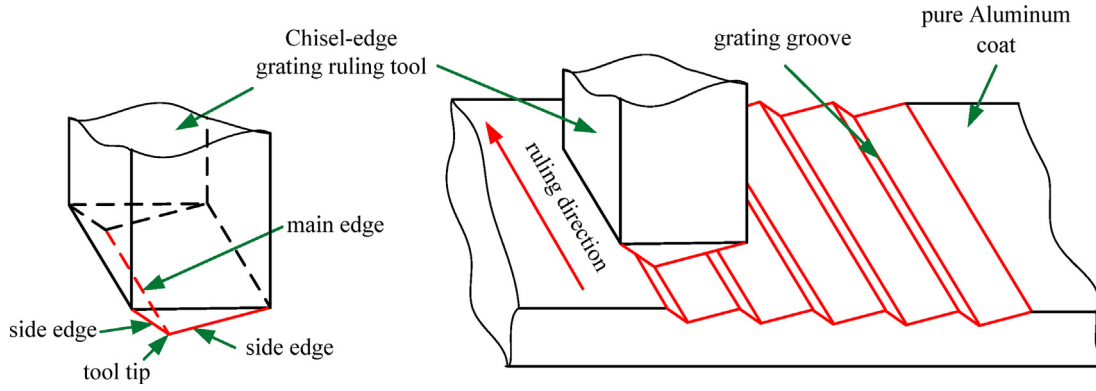
Fig. 1. Schematic view of a chisel-edge ruling tool and the grating ruling process.

groove bottom. An echelle grating with 79 grooves per millimeter, for example, might have a blaze angle of 63.4° and a non-blaze angle of approximately 27°, and correspondingly, the tool geometrical parameters must fit the technical requirements of ruling such a grating. The tool geometry not only determines the groove shape but also affects the quality of the grating. The development of a parameterized tool geometry model and mechanical model is meaningful to the study of the extruding and polishing mechanism of the grating groove.

2. Development of a parameterized mechanical model of diamond tool

The chisel-edge tool structure is presented in Fig. 2. The cross section has an asymmetrical "V" shape, and the main parameters are the tool orientation angle (D), non-orientation angle (F), and back obliquity angle (H). Fig. 2 presents the grating ruling direction, names of important parts of the tool and the geometrical relationship with the coordinate axes. Fig. 2 shows that the main edge of the tool lifts a little in the X–Z plane to form an angle with the X-axis, called the pitching angle (E). The two planes that form the pitching angle are called the orientation plane and non-orientation plane. The other two edges of the tool are formed by the intersections of the back oblique plane with the orientation plane and non-orientation plane and are thus called the orientation side edge and non-orientation side edge. The tool tip (O) is located at the Z-axis of the coordinate system, which is the intersection of the orientation plane, non-orientation plane and back obliquity plane. In developing the parameterized tool model, we see a cross section of the tool on the X–Y plane, as a triangle denoted $\triangle ABC$ in Fig. 2. The three internal angles of the triangle are α, β and λ, where λ is the sum of λ_1 and λ_2, and α is the guide angle of the tool. In the parameterized model of the tool, α is considered a variable while D, F, H, λ, h ($GO = h$), and b ($AC = b$) are constants, and it is set that $AB = c$, $BC = a$, $CO = e$, $CG = L$, $GP_3 = L_1$, $GP_4 = L_2$, h_a ($Gd_1 = h_a$), h_b ($Gd_2 = h_b$), as shown in Fig. 2.

The parameters have the relations

$$\sin(\lambda_1)\tan(D) = \sin(\lambda_2)\tan(F), \tag{1}$$

$$L = L_1 \tan(A_1)/\sin(\lambda_1)\tan(D), \tag{2}$$

$$L_1 = a\cos(\lambda_1) - h/\tan(E), \tag{3}$$

$$a/\sin(\alpha) = b/\sin(\beta) = c/\sin(\lambda). \tag{4}$$

Through above equations and the trigonometry of tool, we can calculate L, E, L_1, A_1, and β. The areas of the three planes of the tool denoted $S_{ABO} = S_H$, $S_{BCO} = S_d$ and $S_{AOC} = S_f$, on the basis of the areas of the planes and the projection areas of the planes on the X–Y plane,

we obtain

$$\sqrt{p(p-a)(p-b)(p-c)}/h = a\cos(D)/(2\sin(D))$$
$$+ b\cos(F)/(2\sin(F)) + c\cos(H)/(2\sin(H)), \tag{5}$$

where $p = (a+b+c)/2$.

Finally, through above equations and the trigonometry of tool, we calculate out parameter a. By similar way letting $Bp_3 = s_1$ and $Ap_4 = s_2$, we can calculate out parameters L_2, A_2, s_1, s_2, B_1, and B_2. Furthermore, based on the previous equations and parameters, we can develop a parameterized tool model.

When a chisel-edge tool extrudes and polishes a film, it experiences the resistance force of the film in the deformation process in the directions of the X, Y, and Z axes. We let pp_a denote the normal pressure on the orientation plane and tt_a denote the shear pressure on the orientation plane, as shown in Fig. 2. The included angles of the normal pressure pp_a and three coordinate axes are denoted x_a, y_a, and z_a. Similar to the case for the normal and shear pressures acting on the orientation plane, pp_b denotes the normal pressure acting on the non-orientation plane while tt_b denotes the shear pressure acting on the non-orientation plane. Tabor suggested that, for a Poisson's ratio of 0.3, the maximum contact pressure at the onset of plastic deformation can be related to the hardness of the softer material, H_n, in the form $pp = 0.6H_n$. Using Tresca's maximum shear stress criterion, we set $tt = H_n/5.65$ [11], and we can obtain the hardness H_n measured by nano-indenter. If the normal and shear pressures acting on each plane are pp and tt, then

$$pp_a = pp_b = pp = 0.6 \times H_n, \tag{6}$$

$$qq_a = qq_b = tt = H_n/5.65. \tag{7}$$

Fig. 2 shows that $z_a = D$. We then obtain x_a from

$$\cos(x_a) = h\cos(D)/L. \tag{8}$$

and obtain y_a from

$$\cos^2(x_a) + \cos^2(y_a) + \cos^2(z_a) = 1. \tag{9}$$

Likewise, considering that $z_b = F$, we can obtain x_b and y_b. S_{dx}, S_{dy} and S_{dz} denote the projections of S_d on the Y–Z, X–Z and X–Y planes respectively. Similarly, S_{fx}, S_{fy} and S_{fz} denote the projections of S_f on the Y–Z, X–Z and X–Y planes respectively. The projection areas are S_{dx} is

$$S_{dx} = S_d \sin(x_a). \tag{10}$$

Likewise, the S_{dy}, S_{dz}, S_{fx}, S_{fy}, and S_{fz} are can be expressed as S_{dx}, p_{xa} and p_{xb} denote the normal pressure distribution in the X direction, p_{ya} and p_{yb} denote the normal pressure distribution in the
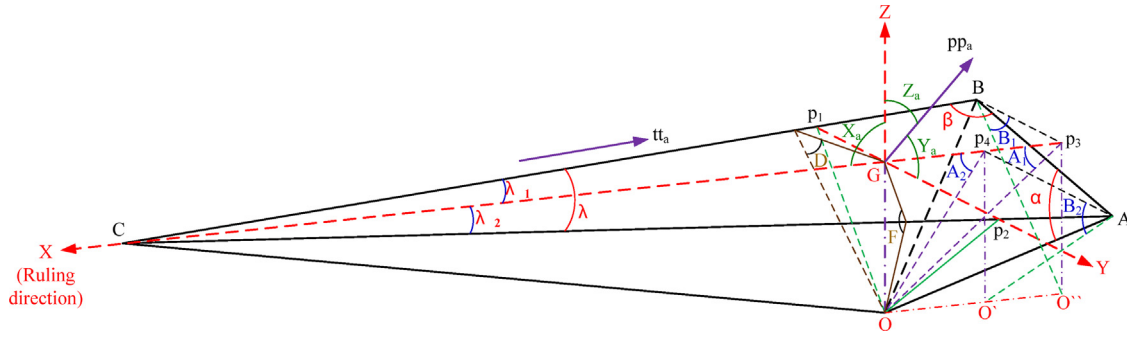
Fig. 2. Parameterized model of the tool.

Y direction, and p_{za} and p_{zb} denote the normal pressure distribution in the Z direction. They can be expressed as following form

$$px_a = pp \cos(x_a). \tag{11}$$

q_{xa} and q_{xb} denote the shear pressure distribution in the X direction, q_{ya} and q_{yb} denote the shear pressure distribution in the Y direction, and q_{za} and q_{zb} denote the shear pressure distribution in the Z direction. They can be expressed as following form

$$qx_a = tt \cos(\lambda_1). \tag{12}$$

P_{xa}, P_{ya} and P_{za} denote the total normal pressure acting on the orientation plane in the X, Y and Z directions, respectively. P_{xb}, P_{yb} and P_{zb} denote the total normal pressure acting on the non-orientation plane in the X, Y and Z directions, respectively. Similarly, the total shear pressure acting on the orientation plane and non-orientation plane in the X, Y and Z directions is expressed as

$$Px_a = px_a S_d, \tag{13}$$

$$Qx_a = qx_a S_d. \tag{14}$$

The sums of pressures acting on the tool in the X, Y and Z directions are respectively denoted Px, Py and Pz and expressed as

$$Px = Px_a + Px_b + Qx_a + Qx_b, \tag{15}$$

$$Py = Py_a - Py_b - Qy_a + Qy_b, \tag{16}$$

$$Pz = Pz_a + Pz_b. \tag{17}$$

Meanwhile, ppx_a, ppy_a and ppz_a denote the unit normal pressure acting on S_{dx}, S_{dy} and S_{dz} (projection areas of the orientation plane), respectively, while ppx_b, ppy_b and ppz_b denote the unit normal pressure acting on S_{fx}, S_{fy} and S_{fz} (projection areas of the non-orientation plane), respectively. Additionally, it is possible to express the unit shear pressure acting on these areas in a similar way, giving

$$ppx_a = Px_a/S_{dx}, \tag{18}$$

$$qqx_a = Qx_a/S_{dx}. \tag{19}$$

On the basis of the force analysis of the tool in the grating ruling process, it is possible to develop a model of the tool torque acting around the Z axis in the grating ruling process. The torque at each point in the projection area in the corresponding (X or Y) direction is calculated, and the algebraic sum of the torque acting on the tool around the Z axis in the grating ruling process is then obtained. For example, by denoting the total torque acting on the projection area (S_{CGO}) of the orientation plane in the Y direction as N_{yaL}, the total torque acting on the tool around the Z axis as N, the total torque produced in the X direction as N_x, and the total torque produced in the Y direction as N_y, we have

$$N_{yaL} = \int_0^L (ppy_a - qqy_a)(L - x)x \, \tan(E)dx, \tag{20}$$

$$N_x = ((qqx_b + ppx_b)s_2^3 \, \tan(B_2) - (qqx_a + ppx_a)s_1^3 \, \tan(B_1))/6, \tag{21}$$

$$\begin{aligned} N_y = &(((ppy_a - qqy_a)L_1^3 \, \tan(A_1) + (ppy_b - qqy_b)L^3 \, \tan(E)) \\ &-((ppy_b - qqy_b)L_2^3 \, \tan(A_2) + (ppy_a - qqy_a)L^3 \, \tan(E)))/6 \end{aligned}, \tag{22}$$

$$N = N_x - N_y. \tag{23}$$

3. Experimental analysis

Based on previous experience of ruling echelles with 79 line/mm, parts of tool parameters, such as $D = 64°$, $F = 26°$, $\lambda = 4.5°$, and $h = 5.4 \, \mu m$ can be determined. In order to validate the proposed tool model, we prepared four tools with back obliquity angle of 10° and different guide angles of 75°, 95°, 115° and 135° respectively. Then, comparison experiments are performed to assess the performances of the four different sets of tool parameters in terms of grating ruling quality. The ruling engine used in the experiments is CIOMP-2 engine in China, and its tool support system consisted of two cross-hinge steel springs. The comparison experiments were carried out on a pure aluminum-coated quartz glass grating substrate with dimensions of $80 \times 100 \times 12 \, mm^3$; the pure aluminum coating thickness was 10.5 μm, the thickness uniformity was better than 0.7%, the surface roughness R_a is 15 nm, and the film hardness measured by nano-indenter H_n is 412 Mpa. We ruled the 79 gr/mm echelle with a blaze angle of 63.43° using four different tool with guide angle of 75°, 95°, 115° and 135° respectively.

When the tool guide angle is 75°, 95°, 115° and 135°, the shapes of real ruled grooves differ. Grooves ruled by a tool with a guide angle of 75°, 95° and 115° appear to be corrugated and not straight, while grooves ruled by a tool with a guide angle of 135° appear to be smooth and straight, as shown in Fig. 3.

We can clearly see the gradual variation of the grating grooves from smooth lines to corrugated lines. The corresponding groove linearity and shape for each of these ruling sections measured by AFM are shown in Fig. 4.

From Fig. 4, we see that the ruled grating grooves are subject to corrugated lines when tool guide angle are 75°, 95°, 115°; when the tool guide angle is 75°, the corrugated lines appear seriously fluctuated line both in longitudinal and transverse directions. When the tool guide angle is 95°, the fluctuating value is decreased, although the fluctuated lines can still be clearly seen to some extent. Then, when the tool guide angle is 115°, the fluctuating value is greatly decreased and becomes hardly clearly seen. Finally, when the tool guide angle is 135°, the grooves appear to be very smooth and straight.

From Fig. 4, we clearly see that each triangle shape of the grooves ruled by tool with guide angle of 75° and 95° are not identical, while each triangle shape of the grooves ruled by tool with guide angle of 115° and 135° are almost similar. And the corresponding surface roughness on blaze plane measured by AFM and groove quality are listed in Table 1, showing that the surface roughness on blaze plane
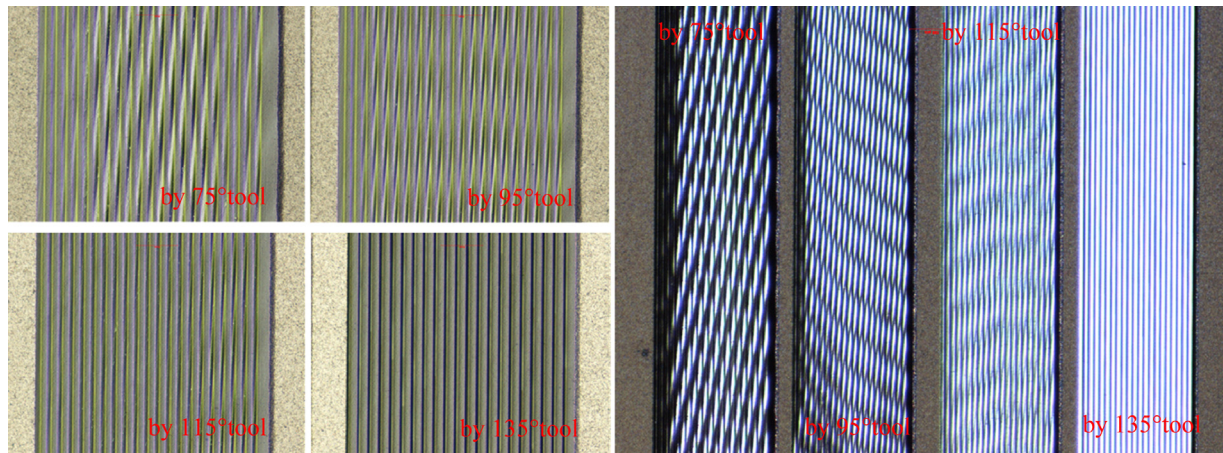
Fig. 3. Groove linearity ruled by a tool with guide angles of 75°, 95°, 115° and 135°.
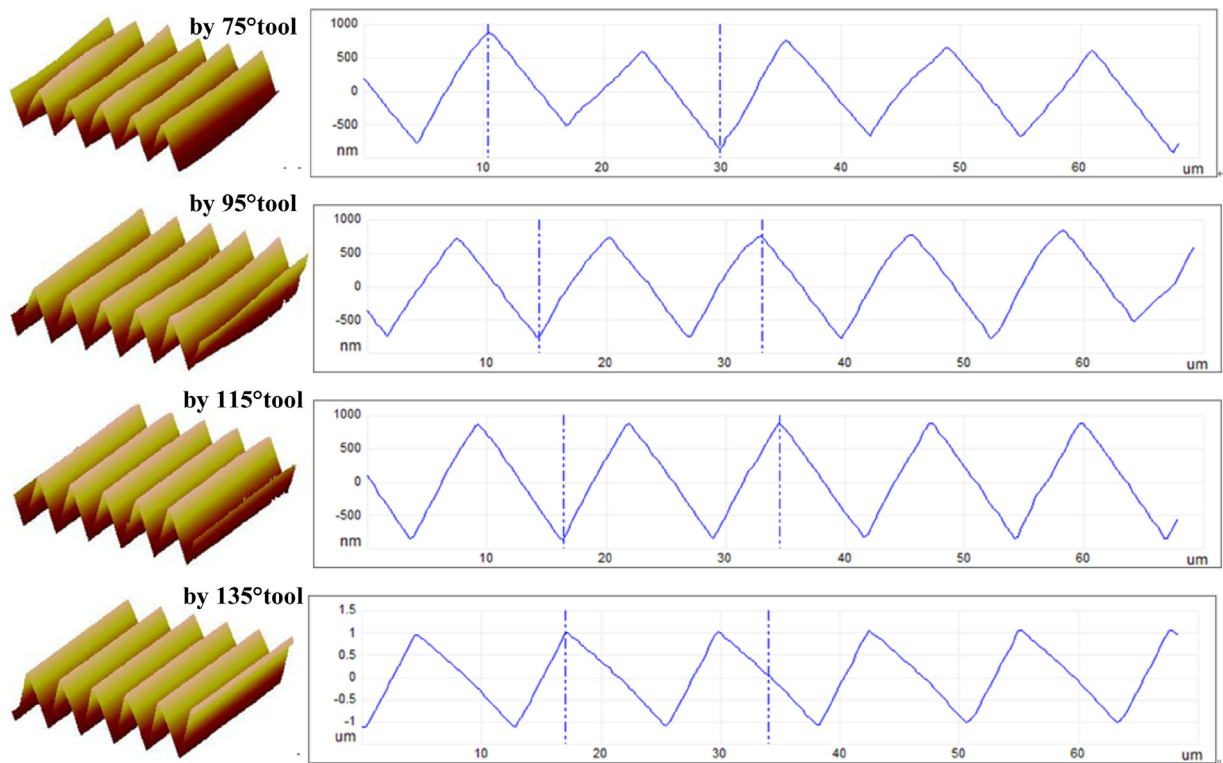

Fig. 4. Groove shapes ruled by a tool with guide angles of 75°, 95°, 115° and 135°.

Table 1
Influence of the guide angles on the ruling accuracy and the surface quality.

Tool guide angle	75°	95°	115°	135°
R_q	8.97 nm	6.24 nm	5.58 nm	5.30 nm
R_a	6.67 nm	4.78 nm	4.61 nm	4.37 nm
Groove shape	worse	worse	better	good
Linearity	worse	worse	better	good

Table 2
Influence of the tool guide angles on the force and torque.

Tool guide angle	75°	95°	115°	135°
Px (N)	0.0722	0.0711	0.0712	0.0733
Py (N)	0.0003	0.0040	0.0082	0.0150
Pz (N)	0.3774	0.3703	0.3697	0.3785
N (Nm)	2.8607×10^{-7}	2.2167×10^{-7}	1.5346×10^{-7}	3.0032×10^{-10}

are gradually reduced while the tool guide angle changes from 75° to 135°.

Based on our proposed tool force and torque model, we can calculate out that total torques of 2.8607×10^{-7} Nm, 2.2167×10^{-7} Nm, 1.5346×10^{-7} Nm and 3.0032×10^{-10} Nm are corresponding to the tool guide angles of 75°, 95°, 115° and 135°. From Table 2, we can see that the torque is gradually reduced from 2.8607×10^{-7} Nm to 3.0032×10^{-10} Nm when the tool guide angle

changes from 75° to 135°. And the tool forces on Z axis calculated by our model are close to the real load on tool in Z axis which is 0.39N.

The experimental results agree well with the theoretical calculation results for torque presented in Table 2. When ruling with a tool guide angle of 75°, 95° and 115°, the torque of the tool exceeds the resistance of the elastic holder, allowing the tool to turn through

a small angle. Finally, the metal coating layer undergoes more of a fluctuating process than a straight ruling process. From the experimental results of grating ruling, we have shown that proposed tool force and torque model can significantly improve both the groove linearity and the groove shape of the resulting echelles.

4. Conclusion

A parameterized mechanical model of a chisel-edge grating ruling tool is developed based on the mechanism of the interaction between the ruling tool and grating film in the grating ruling process. According to the parameterized mechanical model, we can obtain the force and torque value of ruling tool versus the tool guide angle. The comparison experiments were carried out. And we analyzed the corresponding groove linearity, groove shape and surface roughness of blaze plane, and found that the experimental results agree well with the theoretical calculation results for force and torque.

For an echelle grating with 79 grooves per millimeter, when the tool guide angle ranges from 75° to 135°, Px, Py and Pz respectively range 0.0711–0.0733 N, 3.1401e-04–0.015 N and 0.03697–0.03785 N by theoretical calculation. And the real ruling load on tool in Z axis is 0.39N. The theoretical forces and experimental load in the Z directions therefore well match each other. And the tool torque is almost zero for a guide angle of 135° according to theoretical calculation. The calculation was experimentally confirmed that the grating grooves ruled by tool with guide angle of 135° appear smooth and clean.

This illustrates the significance of the parameterized mechanical model when applied between the ruling tool and the grating films for ruling of echelles and gratings, and can provide an important theoretical basis for the design of grating ruling tools. The proposed method is an effective way to solve the corrugated line and fluctuating problems on grating grooves, and can avoid the need for complex and time-consuming technical operations such as step-by-step modification of tool guide angle; this illustrates the significance of our model for practical applications in the ruling of high-performance gratings.

References

[1] Palmer EW, Hutley MC, Franks A, Verrill JF, Gale B. Diffraction gratings. Rep Prog Phys 1975;38:975–1048.
[2] Li Zizheng, Gao Jinsong, Yang Haigui, Wang Tongtong, Wang Xiaoyi. Roughness reduction of large-area high-quality thick Al films for echelle gratings by multi-step deposition method. Opt Express 2015;23:23738–47.
[3] Li Yinghai. Diamond diffraction gratings tool. Opt Precis Eng 1996;4:81–4.
[4] Li Yinghai, Bayanheshig, Xiang-dong QI. The manufacture of ultra-precision diamond tool used the diffraction grating ruling. Microfab Technol Processes 2006;12:15–7.
[5] Yang Haigui, Wang Xiaoyi, Shen Zhenfeng, Gao Jinsong, Zhang Shanwen. Radial-quality uniformity investigations of large-area thick Al films. Opt Eng 2015;54, 045106-1-6.
[6] Harrison George R. The diffraction grating-An opinionated appraisal. Appl Opt 1973;12:2039–49.
[7] Harrison George R. The production of diffraction gratings: II. The design of echelle gratings and spectrographs. J Opt Soc Am 1949;39:522–8.
[8] Verrill JF. Diffraction grating ruling tool alignment by analysis of traced groove profile. J Phys E: Sci Instrum 1975;8:522–5.
[9] Verrill JF. The effects of diamond wear on the production and properties of ruled diffraction gratings. Appar Tech 1982;15:516–9.
[10] Davies DA, Stiff GM. Diffraction grating ruling in Australia. Appl Opt 1969;8:1379–84.
[11] Liu Z, Sun J, Shen W. Study of plowing and friction at the surface of plastic deformed metals. Tribology 2002;35:511–22.